

MEASUREMENT OF THE BLACK HOLE MASS IN NGC 1332 FROM ALMA OBSERVATIONS AT 0.044 ARCSECOND RESOLUTION

AARON J. BARTH¹, BENJAMIN D. BOIZELLE¹, JEREMY DARLING², ANDREW J. BAKER³,
DAVID A. BUOTE¹, LUIS C. HO⁴, JONELLE L. WALSH⁵

Draft version May 5, 2016

ABSTRACT

We present Atacama Large Millimeter/submillimeter Array (ALMA) Cycle 3 observations of CO(2–1) emission from the circumnuclear disk in the E/S0 galaxy NGC 1332 at 0.''044 resolution. The disk exhibits regular rotational kinematics and central high-velocity emission (± 500 km s⁻¹) consistent with the presence of a compact central mass. We construct models for a thin, dynamically cold disk in the gravitational potential of the host galaxy and black hole, and fit the beam-smear model line profiles directly to the ALMA data cube. Model fits successfully reproduce the disk kinematics out to $r = 200$ pc. Fitting models just to spatial pixels within projected $r = 50$ pc of the nucleus (two times larger than the black hole's gravitational radius of influence), we find $M_{\text{BH}} = (6.64^{+0.65}_{-0.63}) \times 10^8 M_{\odot}$. This observation demonstrates ALMA's powerful capability to determine the masses of supermassive black holes by resolving gas kinematics on small angular scales in galaxy nuclei.

Subject headings: galaxies: nuclei — galaxies: bulges — galaxies: individual (NGC 1332) — galaxies: kinematics and dynamics

1. INTRODUCTION

The Atacama Large Millimeter/submillimeter Array (ALMA) has a revolutionary capability to resolve cold molecular gas kinematics on angular scales well below 1''. This opens the possibility of using cold molecular gas disks as dynamical tracers to measure the masses of supermassive black holes (BHs) in galaxy centers (Davis et al. 2013b; Onishi et al. 2015). Accurate measurement of a BH mass (M_{BH}) generally requires observations that resolve kinematics within the BH's gravitational radius of influence r_g , the radius within which the BH dominates the gravitational potential, and ALMA is the first mm/sub-mm interferometer having the capability to resolve r_g in large numbers of galaxies.

NGC 1332 is a nearby S0 or E galaxy that contains a highly inclined circumnuclear dust disk. Its BH mass has been measured previously via stellar dynamics (Rusli et al. 2011) and by modeling the hydrostatic equilibrium of its X-ray emitting halo (Humphrey et al. 2009), making it an excellent laboratory for direct comparison of independent measurement techniques. In Paper I (Barth et al. 2016), we described 0.''3-resolution Cycle 2 ALMA observations designed to test for the presence of CO emission from within r_g . The data showed very clean disklike rotation with a slight warp, and central emission extending to ± 500 km s⁻¹. Our simplest dynamical model fits converged on $M_{\text{BH}} = 6.0 \times 10^8 M_{\odot}$, but beam smearing in the highly inclined disk caused a severe degener-

acy between rotation and turbulent motion at small radii, precluding the derivation of stringent confidence limits on M_{BH} . Here, we present new ALMA Cycle 3 observations at 0.''044 resolution and dynamical modeling of the data. We adopt a distance of 22.3 Mpc to NGC 1332 for consistency with Paper I and with Rusli et al. (2011); at this distance, 1'' corresponds to 108.6 pc.

2. OBSERVATIONS

NGC 1332 was observed in ALMA Band 6 as part of project 2015.1.00896.S. Three separate observations on 2015 September 16 and 23 were carried out, for a total on-source integration time of 101 min. The observations were obtained in a frequency band centered at 229.354 GHz, corresponding to the redshifted ¹²CO(2–1) line in NGC 1332. We processed the data using the Common Astronomy Software Applications (CASA; McMullin et al. 2007) package to produce an emission-line data cube with 0.''01 pixels, a field of view of 6.''4 × 6.''4, and 75 frequency channels with a channel spacing of 15.4 MHz, corresponding to a velocity width of 20.1 km s⁻¹ per channel for the CO(2–1) line. The synthesized beam has major and minor axis FWHM sizes of 0.''052 and 0.''037 with major axis position angle (PA) 64°, giving a geometric mean resolution of 0.''044.

We created kinematic maps by fitting Gaussian line profiles to the data. In order to increase the S/N of the profile fits, we first binned the data cube spatially by block averaging in 4 × 4 pixel blocks, producing 0.''04 pixels. The CO intensity, line-of-sight mean velocity (v_{LOS}), and width (σ_{LOS}) are shown in Figure 1. The disk kinematics are illustrated over an elliptical region with major and minor axes of 3.''7 and 0.''5, corresponding to the largest region over which we were able to obtain successful profile fits at each binned pixel. At the 0.''04 binned pixel scale, the rms noise level is 0.142 mJy beam⁻¹ per channel, and the median S/N per 0.''04 spatial pixel is 7.2 over this elliptical region. The v_{LOS} map illustrates remarkably regular disklike rotation, with subtle signs of the mild kinematic twist or warp we found in the Cycle 2

¹ Department of Physics and Astronomy, 4129 Frederick Reines Hall, University of California, Irvine, CA. 92697-4575, USA; barth@uci.edu

² Center for Astrophysics and Space Astronomy, Department of Astrophysical and Planetary Sciences, University of Colorado, 389 UCB, Boulder, CO 80309-0389, USA

³ Department of Physics and Astronomy, Rutgers, the State University of New Jersey, 136 Frelinghuysen Road, Piscataway, NJ 08854-8019, USA

⁴ Kavli Institute for Astronomy and Astrophysics, Peking University, Beijing 100871, China; Department of Astronomy, School of Physics, Peking University, Beijing 100871, China

⁵ George P. and Cynthia Woods Mitchell Institute for Fundamental Physics and Astronomy, Department of Physics and Astronomy, Texas A&M University, College Station, TX 77843-4242, USA

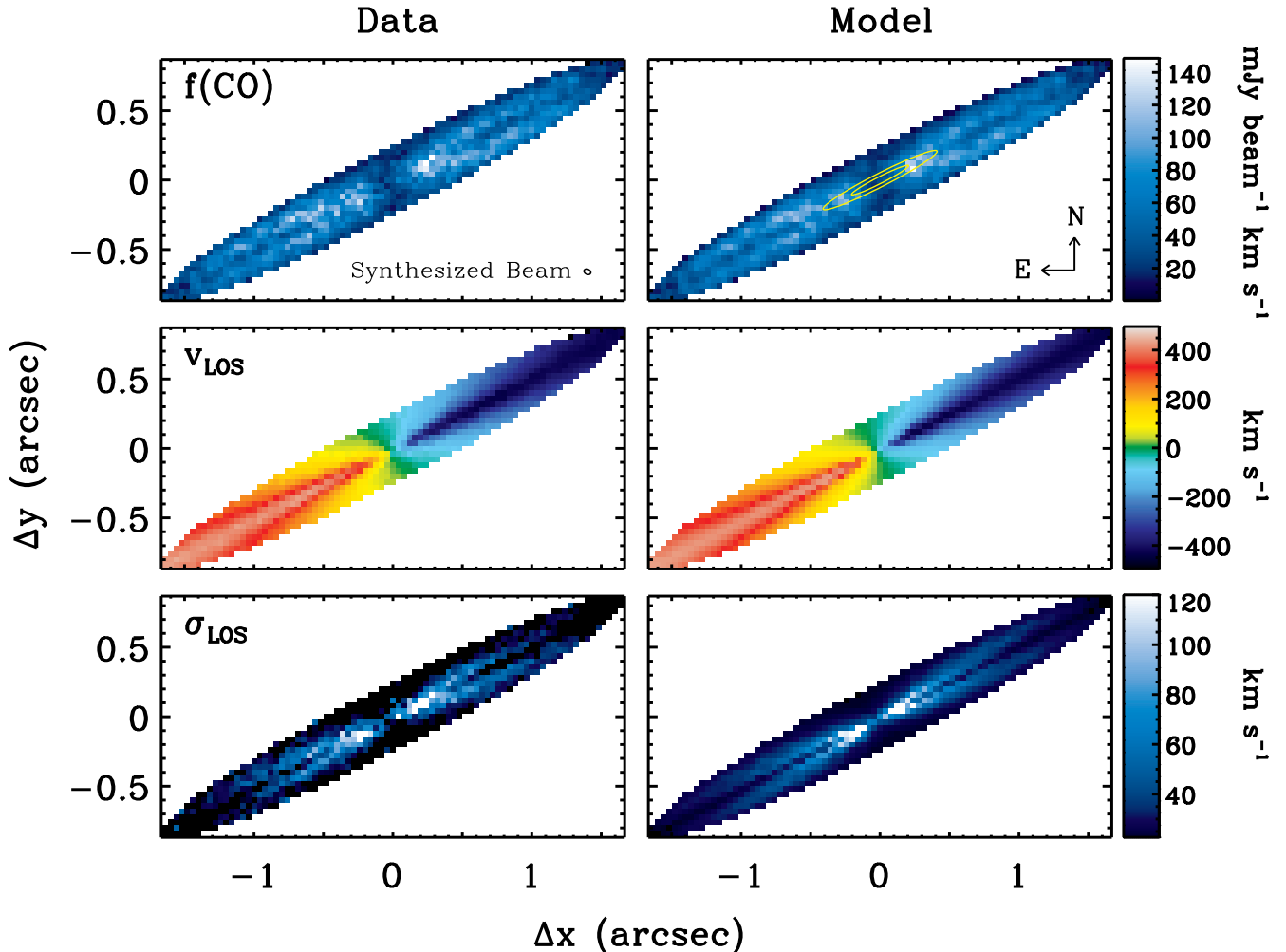


FIG. 1.— Maps of CO(2–1) intensity, v_{LOS} (relative to $v_{\text{sys}} = 1562 \text{ km s}^{-1}$), and σ_{LOS} in $0''.04$ binned pixels for the data and best-fitting full-disk model. In the top right panel, the yellow ellipses denote the projected BH sphere of influence ($r_{\text{g}} = 25 \text{ pc}$), and the $r_{\text{fit}} = 50 \text{ pc}$ region used for our final fits.

data. In the σ_{LOS} map, the “X” shaped feature is characteristic of rotational broadening in an inclined disk. The major axis position-velocity diagram (PVD) exhibits a central velocity upturn to $\approx 500 \text{ km s}^{-1}$ (Figure 2), similar to that seen in the Cycle 2 data.

3. DYNAMICAL MODELING

Our dynamical modeling follows the methods described in Paper I. We model a thin disk in circular rotation in a gravitational potential containing a central point mass and an extended mass distribution from stars. The enclosed stellar mass $M_*(r)$ is based on a deprojected luminosity profile $L_*(r)$ multiplied by a mass-to-light ratio Υ . We neglect the contributions of dark matter and of molecular gas, both of which are $\lesssim 10^8 M_{\odot}$ within $r = 250 \text{ pc}$; in contrast, $M_*(250 \text{ pc}) \approx 10^{10} M_{\odot}$ (Paper I). Models are computed on a spatial grid with $0''.01$ pixels. At each grid element, we determine the line-of-sight component of the disk’s rotation velocity (relative to the systemic velocity v_{sys}), observed at inclination i and major axis position angle Γ . The emission line at each grid point is assumed to have a Gaussian velocity profile, with turbulent velocity dispersion σ_{turb} .

This procedure produces a simulated cube with the same velocity channel spacing as the data cube. The total line flux

at each spatial element is scaled to match a CO surface brightness map measured from the ALMA data. Then, each velocity channel image in the model is convolved with the ALMA synthesized beam, and the model is rebinned to match the $0''.04$ spatial scale of the binned ALMA data cube. The goodness of fit (quantified by χ^2) is computed by direct comparison of the model cube with the binned ALMA data. Calculating χ^2 at a spatial scale of approximately one pixel per synthesized beam substantially mitigates the problem of spatially correlated noise in the data, which would be a significant issue if χ^2 were computed for $0''.01$ pixels (see Paper I). Free parameters include M_{BH} , Υ , σ_{turb} , i , Γ , v_{sys} , the dynamical center position (x_0, y_0) , and an overall normalization factor f_0 applied to the CO surface brightness model. We assume a uniform value of σ_{turb} over the disk surface and discuss this assumption in §4.3. We optimize the model fits using the amoeba downhill simplex method in IDL.

To model $M_*(r)$, we use the deprojected stellar luminosity profile from Rusli et al. (2011), based on a combination of K -band VLT adaptive-optics data at small radii ($r < 4''.5$) and R -band imaging at larger radii. Their best-fitting stellar-dynamical model implies an R -band mass-to-light ratio of $\Upsilon_R = 7.35$ (J. Thomas, private communication). Rusli et al.

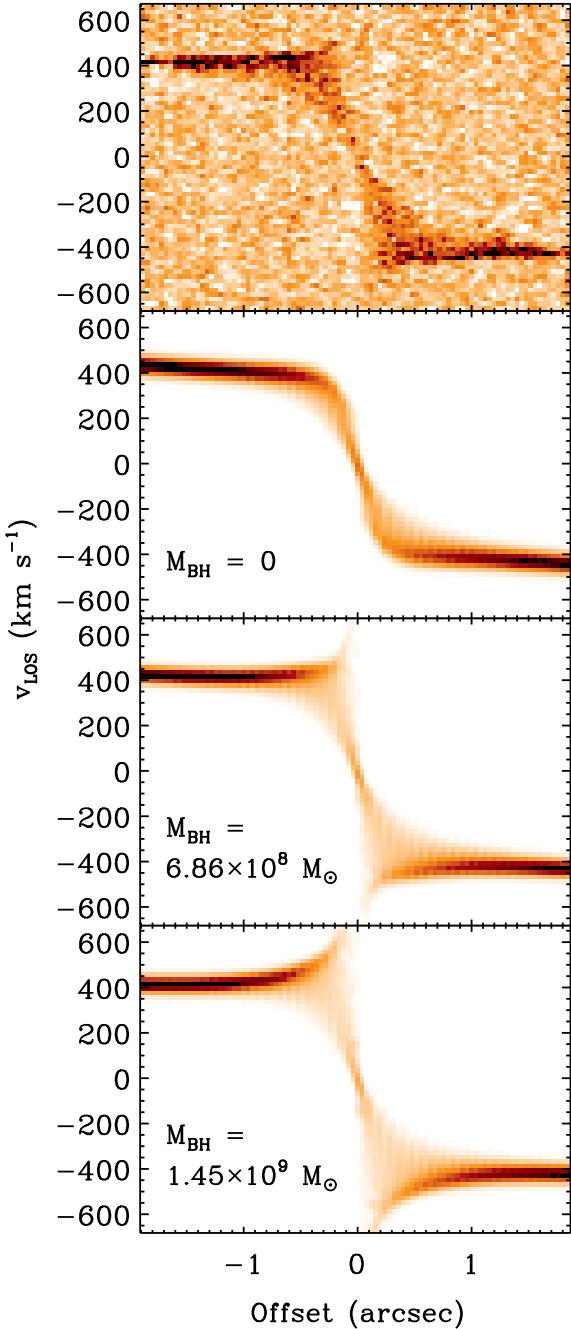


FIG. 2.— PVDs generated by rotating the data cubes clockwise by 27° and extracting a single-pixel ($0''.04$) cut along the disk major axis. *Top panel:* Observed PVD. *Lower panels:* PVDs from full-disk model fits with M_{BH} fixed at 0, $6.86 \times 10^8 M_\odot$ (the best-fitting mass for the full-disk model fit), and $1.45 \times 10^9 M_\odot$ (as measured by Rusli et al. 2011). The model PVDs are recomputed using a flat, noise-free CO surface brightness profile rather than the observed surface brightness profile, in order to illustrate the disk kinematics more clearly. The broad velocity spread at small radii is the result of beam smearing of unresolved rotation.

(2011) give full details of the $L_*(r)$ measurement, and Paper I presents a plot of $M_*(r)$.

4. MODELING RESULTS

4.1. Fits to the full disk

We first describe models fitted to the entire disk, over the elliptical region illustrated in Figure 1. This region contains 840 binned ($0''.04$) spatial pixels. We compute χ^2 over 56 frequency channels, for a total of 47040 data points. With all model parameters free, the best fit is found at $M_{\text{BH}} = 6.86 \times 10^8 M_\odot$, with $\chi^2_{\text{min}} = 55206.9$ or $\chi^2_\nu = 1.17$. Other parameters for the best-fitting model are $\Upsilon_R = 7.53$, $i = 84^\circ 1$, $\Gamma = 117^\circ 2$, and $\sigma_{\text{turb}} = 22.2 \text{ km s}^{-1}$; these are similar to the best-fitting values found in Paper I. Figure 3 shows $\Delta\chi^2 = \chi^2 - \chi^2_{\text{min}}$ as a function of M_{BH} . The 68.3% confidence region (corresponding to $\Delta\chi^2 = 1$) is $(6.86 \pm 0.14) \times 10^8 M_\odot$. Kinematic maps measured from the best-fitting model (Figure 1) match the structure in the data closely. While the model is generally successful at reproducing the disk kinematics, a result of $\chi^2_\nu = 1.17$ for 47032 degrees of freedom is formally unacceptable. We attribute this to systematic inadequacies of the model, such as neglect of the disk’s slight warp, the assumption of a spatially constant value of σ_{turb} , and noise in the CO surface brightness model.

The apparently high precision of this result is typical of gas-dynamical models fitted to a large number of pixels (Gould 2013). However, the model-fitting (statistical) uncertainties only represent a portion of the true error budget for the full-disk fits. In this case, the major source of systematic uncertainty is likely to be the stellar mass profile. Pixels at $r \gg r_g$ in the ALMA data dominate the full-disk fit, leading to very tight constraints on Υ and consequently on M_{BH} as well. If the assumed stellar mass profile shape is systematically wrong, model fits will force M_{BH} to an incorrect (but ostensibly precise) value.

4.2. Fits to smaller regions

The stellar mass profile can be incorporated into the error budget on M_{BH} if the uncertainty in its shape can be parameterized, with addition of one or more free parameters to the model. Potential sources of error in the mass profile shape include errors due to dust extinction, errors in deprojection from two to three dimensions, and Υ gradients due to stellar population age and/or metallicity variations (McConnell et al. 2013). Properly accounting for this range of uncertainties over the entire radial range of the disk would be challenging.

The alternative and simpler approach is to fit models over only spatial pixels close to and within r_g , so that the BH accounts for a larger fraction of the total enclosed mass. This makes the model-fitting results less susceptible to errors due to the shape of the stellar mass profile, and will appropriately broaden the confidence range on M_{BH} since Υ will be less tightly constrained. Fits to smaller regions can also mitigate systematic mismatch of flat-disk models to the disk’s slightly warped structure. Our goal is to fit models over the smallest possible spatial region that permits successful fits with well-defined confidence limits on M_{BH} (manifested by a smooth and regular curve of χ^2 vs. M_{BH}).

We fit models to progressively smaller regions centered on the nucleus and bounded by ellipses with semimajor and semiminor axis lengths of r_{fit} and $r_{\text{fit}} \cos 84^\circ$, for varying values of r_{fit} (where the full disk corresponds to $r_{\text{fit}} = 200 \text{ pc}$). The curve of χ^2 vs. M_{BH} begins to show asymmetric structure for $r_{\text{fit}} \leq 75 \text{ pc}$ (Figure 3), becoming increasingly irregular and jagged for $r_{\text{fit}} \leq 50 \text{ pc}$ due to the small number of pixels and relatively low S/N in the fitting region. The irregular structure in the χ^2 curve is primarily the result of small fluctuations in the best-fitting values of x_0 , y_0 , and v_{sys} for different fixed val-

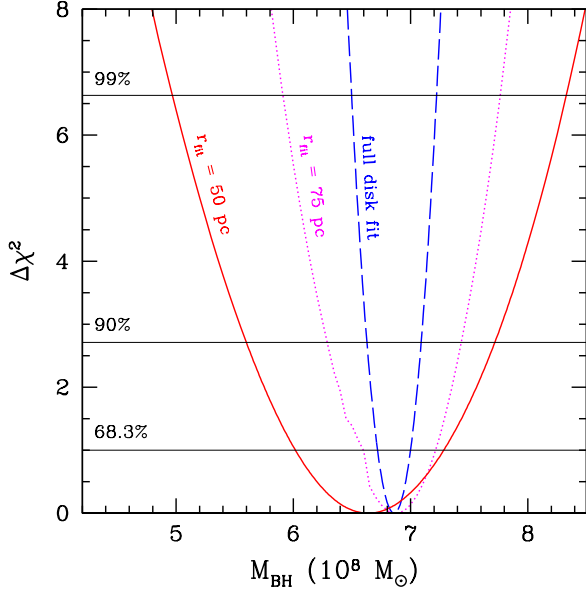


FIG. 3.— Plot of $\Delta\chi^2 = \chi^2 - \chi_{\min}^2$ for fits to the full disk ($r_{\text{fit}} = 200$ pc), $r_{\text{fit}} = 75$ pc with all parameters free (other than M_{BH}) at each trial value of M_{BH} , and $r_{\text{fit}} = 50$ pc with x_0 , y_0 , and v_{sys} fixed.

ues of M_{BH} . From the best-fitting model with $r_{\text{fit}} = 50$ pc, we take the values of these three parameters and hold them fixed, calculating a grid of models with $r_{\text{fit}} = 50$ pc for a range of values of M_{BH} with the remaining five parameters free.

These constrained fits for $r_{\text{fit}} = 50$ pc (containing 45 spatial pixels) have 2515 degrees of freedom, and the best-fitting model has $\chi^2 = 2739.8$ and $\chi_{\nu}^2 = 1.09$. The expected range on χ_{ν}^2 for 2515 degrees of freedom is 1.00 ± 0.03 , so this result suggests that there is still a mild degree of systematic model-data mismatch within $r_{\text{fit}} = 50$ pc. The 68.3% and 99% confidence ranges on M_{BH} are $(6.64^{+0.65}_{-0.63}) \times 10^8$ and $(6.64^{+1.69}_{-1.66}) \times 10^8 M_{\odot}$, respectively. Other parameters of the best-fitting model are $\Upsilon_R = 7.83$ (giving $M_{\star} = 1.8 \times 10^9 M_{\odot}$ within $r_{\text{fit}} = 50$ pc), $i = 85^{\circ}.2$, $\Gamma = 116^{\circ}.7$, and $\sigma_{\text{turb}} = 32.1$ km s $^{-1}$; the fixed value of v_{sys} is 1562.2 km s $^{-1}$. The error budget does not incorporate uncertainty in the distance to NGC 1332; the derived M_{BH} scales linearly with the assumed distance. The fits rule out $M_{\text{BH}} = 0$ at $> 99.99\%$ confidence ($\Delta\chi^2 = 74$ relative to the best-fitting M_{BH}). We interpret the systematic changes in i and Γ for smaller fitting regions as indications of the disk’s warp; these angles vary by only $\sim 1^{\circ}$ from $r_{\text{fit}} = 200$ pc down to $r_{\text{fit}} = 50$ pc or smaller regions. This model implies $r_g = 25$ pc or $0''.23$, determined as the radius within which $M_{\star}(r_g) = M_{\text{BH}}$. Along the disk’s minor axis, this projects to $r_g \cos i = 0''.02$.

For $r_{\text{fit}} < 50$ pc, the χ^2 curve again becomes irregular and asymmetric, even with x_0 , y_0 , and v_{sys} held fixed. Achieving stable fits for $r_{\text{fit}} < 50$ pc is possible if the values of i , Γ , σ_{turb} , and/or f_0 are fixed, but we choose $r_{\text{fit}} = 50$ pc for our final results since it is the smallest region over which we can obtain successful fits with all of these parameters free, and because χ_{ν}^2 increases slightly for values of r_{fit} smaller than 50 pc.

4.3. Turbulent velocity dispersion

In Paper I, we carried out fits using a spatially uniform σ_{turb} , and also ran models allowing for a central rise in σ_{turb} . The models allowing more flexibility in $\sigma_{\text{turb}}(r)$ strongly preferred

the presence of a steep increase in σ_{turb} at small radius, reaching high (and likely unphysical) values of up to 270 km s $^{-1}$ while driving M_{BH} to zero. The fundamental problem was that the extreme beam smearing due to the disk’s high inclination produced very broad line profiles near the disk center, and the model fits were unable to distinguish between rapid rotation and turbulent broadening at small radii.

The Cycle 3 data are much less susceptible to this particular degeneracy, but with $r_g \cos i = 0''.02$ the minor-axis kinematics are still unresolved by a factor of two, leading to significant beam smearing of line profiles at small r . This blurring is evident in the PVD as the “fan” of emission across a broad velocity range at small radii (Figure 2), and as the “X”-shaped rise in the σ_{LOS} map (Figure 1). This velocity structure is well matched by our models with uniform (and low) values of σ_{turb} ; a high central σ_{turb} is not required in order to match the central increase in the observed σ_{LOS} .

In our best-fit model with $r_{\text{fit}} = 50$ pc, for which $\sigma_{\text{turb}} = 32.1$ km s $^{-1}$, the maximum value of $\sigma_{\text{turb}}/v_{\text{rot}}$ is 0.073, small enough to justify our treatment of the disk as dynamically cold and geometrically thin. The $r_{\text{fit}} = 50$ pc model suggests a modest central increase in σ_{turb} relative to the outer disk, where our full-disk fit found $\sigma_{\text{turb}} = 22.2$ km s $^{-1}$. We carried out trial fits to smaller regions of $r_{\text{fit}} = 40$ or 30 pc and found that σ_{turb} never exceeded 40 km s $^{-1}$ for best-fitting models over any fitting region. This demonstrates that the Cycle 3 data do not require or prefer a high central σ_{turb} .

5. DISCUSSION AND CONCLUSIONS

This work presents the first BH mass derived from ALMA observations that resolve the BH’s gravitational radius of influence, demonstrating ALMA’s powerful capability to improve our understanding of local BH demographics. The primary challenges for gas-dynamical measurements of BH masses are identifying disks that exhibit suitably clean rotation, and obtaining observations of sufficient angular resolution and S/N to map the kinematics on the required scales. While a great deal of effort has been invested in measurement of ionized gas kinematics, primarily with *Hubble Space Telescope* spectroscopic observations, the cold molecular gas in circumnuclear disks is known to be less turbulent than the ionized component, making molecular kinematics a more accurate tracer of a galaxy’s gravitational potential than optical emission-line kinematics (Young et al. 2008; Davis et al. 2013a). Resolving r_g in CO observations of nearby galaxies was at the limiting edge of the capabilities of earlier mm-wave interferometers (Davis et al. 2013b), but ALMA will be able to carry out such observations for a large number of galaxies.

In Paper I we stressed the importance of resolving angular scales corresponding to $r_g \cos i$ (the BH radius of influence projected along the disk’s minor axis) in order to fully resolve disk kinematics within the BH’s sphere of influence. This Cycle 3 observation of NGC 1332 fully resolves r_g , but $r_g \cos i$ is unresolved by a factor of two. Thus, the observed kinematics are still blurred by beam smearing in the minor-axis direction, as seen in the σ_{LOS} map and the PVD, but this effect is far less severe than in our Cycle 2 observation. Higher resolution observations would be required in order to determine the disk’s central $\sigma_{\text{turb}}(r)$ profile accurately and reduce the remaining degeneracy between rotation and turbulence in the inner disk. This would permit even tighter constraints on M_{BH} and provide unique information on the physical properties of molecular gas deep within the gravitational potential well of a supermassive BH.

The ideal situation for a gas-dynamical BH mass measurement is achieved when observations have sufficiently high S/N and angular resolution that M_{BH} can be well constrained by models fitted only to points within $r < r_g$, so that stellar mass represents a small contribution to the total enclosed mass and systematic uncertainties in the stellar mass profile have a negligible impact on the measurement. This has previously been accomplished for a few objects using ionized gas kinematics (e.g. M87; Macchetto et al. 1997; Walsh et al. 2013) as well as for H₂O maser disk galaxies such as NGC 4258 (Miyoshi et al. 1995; Kuo et al. 2011). ALMA is certainly capable of achieving this goal for observations of CO or other molecular tracers. With an optimal combination of high angular resolution and S/N, ALMA observations of other targets could in principle provide BH mass precision at the level of a few percent in future measurements. All else being equal, the most precise BH masses will be determined from observations of disks at intermediate inclination angles satisfying the competing requirements that $r_g \cos i$ is resolved and $v \sin i$ is large enough to permit accurate kinematic mapping. NGC 1332 is a challenging target in that the high disk inclination requires observations at very high angular resolution. At high resolution the S/N per spatial pixel is low, and for this measurement, S/N is the primary limiting factor for determining M_{BH} . Significant improvement in S/N would require a very large investment of ALMA time, however, far more than the ~ 5 hours (including calibrations and overhead time) used for this observation.

The CO kinematics are highly inconsistent with a central mass as high as $M_{\text{BH}} = (1.45 \pm 0.20) \times 10^9 M_{\odot}$, the value found by Rusli et al. (2011) based on stellar-dynamical modeling of VLT adaptive-optics spectroscopic data. For our constrained fits with $r_{\text{fit}} = 50$ pc, we find $\Delta\chi^2 = 101$ at $M_{\text{BH}} = 1.45 \times 10^9 M_{\odot}$, and $\Delta\chi^2 = 67$ for $M_{\text{BH}} = 1.25 \times 10^9 M_{\odot}$. This disagreement is particularly stark in that we are using the same stellar luminosity profile measured by Rusli et al. (2011) in our dynamical models, and our fits find a stellar mass-to-light ratio very similar to their best-fit value. It would be worthwhile to revisit the stellar-dynamical models for NGC 1332 to determine whether this disagreement can be resolved.

Our best-fitting BH mass is consistent with the value $5.2_{-2.8}^{+4.1} \times 10^8 M_{\odot}$ (90% confidence) found by Humphrey et al. (2009) from modeling the hydrostatic equilibrium of the dif-

fuse X-ray emitting hot gas halo of NGC 1332. This agreement provides new motivation to explore the hydrostatic equilibrium method as a promising approach for measurement of the central mass profiles in elliptical galaxies and to carry out additional direct comparisons with other mass measurement techniques.

The scatter in the $M_{\text{BH}} - \sigma_*$ correlation at low redshift provides a fossil record of the cosmic history of BH evolution through accretion and mergers (Robertson et al. 2006; Peng 2007). Determination of this scatter requires a large sample of M_{BH} measurements with reliable measurement uncertainties. The factor of two disagreement between our gas-dynamical M_{BH} value and the stellar-dynamical result from Rusli et al. (2011) serves as an important cautionary note regarding the measurement and interpretation of the scatter in the $M_{\text{BH}} - \sigma_*$ relation, which is primarily determined from stellar-dynamical measurements (Gültekin et al. 2009; McConnell & Ma 2013; Kormendy & Ho 2013). Our results suggest that much more effort will be required in order to arrive at a definitive empirical understanding of the scatter in the local BH-bulge correlations. ALMA is poised to make a major contribution to our understanding of local BH demographics, if significant numbers of cleanly rotating molecular disks similar to the NGC 1332 disk can be identified.

This paper makes use of data from ALMA program 2015.1.00896.S. ALMA is a partnership of ESO (representing its member states), NSF (USA) and NINS (Japan), together with NRC (Canada) and NSC and ASIAA (Taiwan), in cooperation with the Republic of Chile. The Joint ALMA Observatory is operated by ESO, AUI/NRAO and NAOJ. The National Radio Astronomy Observatory is a facility of the National Science Foundation operated under cooperative agreement by Associated Universities, Inc. We thank Jens Thomas for providing the stellar mass profile from Rusli et al. (2011).

LCH acknowledges support from the Chinese Academy of Science through grant XDB09030102 (Emergence of Cosmological Structures) from the Strategic Priority Research Program, and from the National Natural Science Foundation of China through grant 11473002.

Facilities: ALMA

REFERENCES

- Barth, A. J., Darling, J., Baker, A. J., Boizelle, B. D., Buote, D. A., Ho, L. C., & Walsh, J. L. 2016, *ApJ*, in press (arXiv:1603.04523).
- Davis, T. A., Alatalo, K., Bureau, M., et al. 2013a, *MNRAS*, 429, 534
- Davis, T. A., Bureau, M., Cappellari, M., Sarzi, M., & Blitz, L. 2013b, *Nature*, 494, 328
- Gould, A. 2013, arXiv:1303.0834
- Gültekin, K., Richstone, D. O., Gebhardt, K., et al. 2009, *ApJ*, 698, 198
- Humphrey, P. J., Buote, D. A., Brighenti, F., Gebhardt, K., & Mathews, W. G. 2009, *ApJ*, 703, 1257
- Kormendy, J., & Ho, L. C. 2013, *ARA&A*, 51, 511
- Kuo, C. Y., Braatz, J. A., Condon, J. J., et al. 2011, *ApJ*, 727, 20
- Macchetto, F., Marconi, A., Axon, D. J., et al. 1997, *ApJ*, 489, 579
- McConnell, N. J., Chen, S.-F. S., Ma, C.-P., et al. 2013, *ApJ*, 768, L21
- McConnell, N. J., & Ma, C.-P. 2013, *ApJ*, 764, 184
- McMullin, J. P., Waters, B., Schiebel, D., Young, W., & Golap, K. 2007, *Astronomical Data Analysis Software and Systems XVI*, 376, 127
- Miyoshi, M., Moran, J., Herrnstein, J., et al. 1995, *Nature*, 373, 127
- Onishi, K., Iguchi, S., Sheth, K., & Kohno, K. 2015, *ApJ*, 806, 39
- Peng, C. Y. 2007, *ApJ*, 671, 1098
- Robertson, B., Hernquist, L., Cox, T. J., et al. 2006, *ApJ*, 641, 90
- Rusli, S. P., Thomas, J., Erwin, P., et al. 2011, *MNRAS*, 410, 1223
- Walsh, J. L., Barth, A. J., Ho, L. C., & Sarzi, M. 2013, *ApJ*, 770, 86
- Young, L. M., Bureau, M., & Cappellari, M. 2008, *ApJ*, 676, 317-334